

# Predicting Blown Film Residual Stress Levels Influence on Properties

Thomas I. Butler  
Blown Film Technology, LLC  
Lake Jackson, TX 77566  
tbutler@blownfilmtech.com

## ABSTRACT

The blown film process extrudes polymer melt from the extruder through an annular die where the bubble is inflated and drawn in the machine and cross directions while being cooled by an air ring system. The extension and cooling play critical roles in this process, directly affecting the residual stress level developed. The residual stress can significantly influence film properties. A new extensional viscosity model was developed to predict the stress developed in the bubble. The bubble cooling effects and crystallization were characterized along the bubble. The results are correlated to changes measured in film properties. How the processing conditions can be modified to provide improved film properties will be discussed.

### Output rate

The extruder size, screw design, screw speed, barrel zone temperatures, polymer design, and backpressure of the die (for smooth barrel extruders) all combine to determine the output rate of an extruder/screw. The output rate from a blown film die can be calculated using Equation (1). For a given polymer density ( $\rho_s$ ) producing a specified bubble size ( $r_f$ ) and thickness ( $h_f$ ), then the haul-off velocity will increase linearly with increasing output rate.

(1) **Output rate from a blown film die.**

$$M = (2 * \pi * r_f * h_f * \rho_s) * V_f \quad M/t$$

The output rate of two blown film lines with different die diameters can be compared, using die specific output rate (DSO). There are different ways of expressing the DSO. Europe uses DSO expressed as kg/hr/mm of die diameter (Equation (3)). North America uses DSO expressed as pounds/hour/inch of die circumference (Equation (2)). The DSO is used to scale-up output rates for different die sizes, if a similar bubble cooling system is used.

(2) **DSO (North America)**

$$\frac{M}{(D * \pi)} \quad \text{lb/hr/in-c} \quad M/t * L$$

(3) **DSO (Europe)**

$$\frac{M}{D} \quad \text{kg/hr/mm-d} \quad M/t * L$$

The Deborah number ( $De$ ) is defined in Equation (4). The Deborah is a dimensionless parameter used to relate the polymer extensional relaxation time to a characteristic process time.  $De$  is a critical parameter in predicting draw resonance bubble instability.

(4) **Deborah number**

$$De = \frac{\lambda_e * V_o}{FLH}$$

The Aspect ratio ( $A$ ) is defined in Equation (5). The Aspect ratio is a dimensionless number that relates the geometry of the bubble and die.  $De$  is also a parameter used in predicting bubble instability.

(5) Aspect Ratio

$$A = \frac{FLH}{r_o}$$

**Bubble Forming**

Figure - 1 shows the forces applied on the blown film process when air is used to inflate a trapped bubble to the desired layflat. The internal bubble pressure ( $\Delta P$ ) expands the molten polymer in the hoop direction or cross direction (CD). The final radius of the bubble is the result of the work done by the expanding force supplied by the  $\Delta P$  (excluding the expansion from the Bernoulli Effect in the air ring cone). The internal bubble pressure typically ranges from 12 to 75 Pa (0.05 to 0.3 inch of H<sub>2</sub>O). The nip rolls supply the haul-off force ( $F_{\text{haul-off}}$ ) to deform the bubble in the MD. The haul-off force is more difficult to measure on a blown film line. The haul-off force varies from 2.2 to 45 N (0.5 to 10 lb<sub>f</sub>). The haul-off force is uniformly applied across the bubble cross sectional area up and down the bubble.

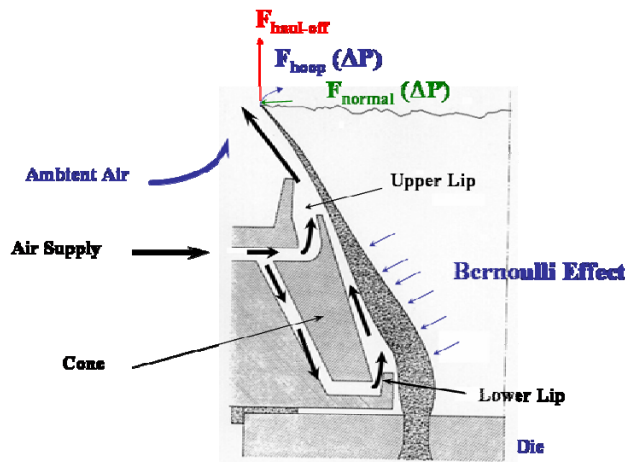


**Figure - 1 Forces acting on the blown film bubble.**

The blown film process uses dimensionless ratios to describe to the forming of the bubble. The basic ratios of blown film are blow-up ratio (BUR) for the CD extension and draw-down ratio (DDR) for MD extension.

The BUR as defined by Equation (6) is an indicator of the amount of expansion (strain) in the bubble in the cross direction (CD). BUR does not describe the total strain or the strain rate.

$$(6) \quad BUR = \frac{r_f}{r_o}$$

The DDR as shown in Equation (7) is an indicator of the elongation (strain) that occurs in the MD. The definition is the ratio of velocity of the haul-off to the velocity at the die exit. DDR does not describe the total strain or the strain rate.

$$(7) \quad DDR = \frac{V_f}{V_o}$$

Air rings are designed to cool the melt and stabilize it. Air ring technology involves two important aerodynamic phenomenons:

(1) The Bernoulli Effect (also known as Venturi effect) where a pressure drop is created when a fluid velocity (air) is accelerated due to a reduction in the flow cross sectional area.

(2) The Coanda Effect is a vortex flow field that forms when a free fluid flow attaches to a surface and flows along the surface.

The Bernoulli Effect occurs in the air ring when a fluid (air) flows into a restricted area resulting in the increase of air velocity which creates a pressure drop in the flow area as shown in Figure -2.

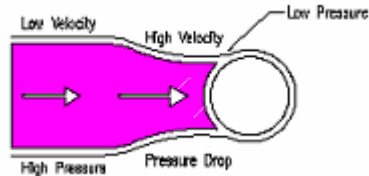


Figure – 2 Bernoulli Effect occurs when air velocity is accelerated and causes the pressure to decrease.

The Bernoulli Effect in blown film occurs when the lower pressure generated by a high velocity air flow is applied to the free surface of the bubble, causing the bubble to be pulled out, as shown in Figure – 3. Polymers with very high melt strength require higher air velocities to produce sufficient pressure drop to pull the bubble surface toward the cone surface. Polymers with low melt strength, such as LLDPE, greatly benefit from the Bernoulli Effect of dual lip air rings, because output rates of these polymers can be significantly increased.

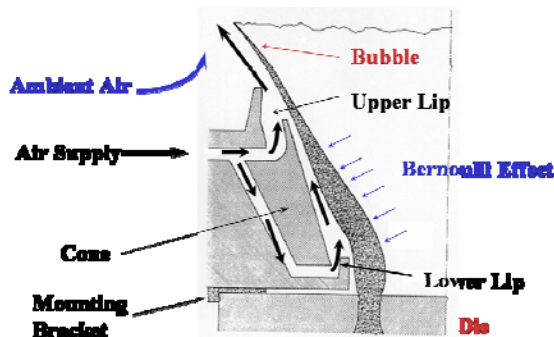


Figure – 3 The Bernoulli Effect occurs in a dual lip air ring pulling the bubble close to the forming cone.

### Dual-orifice Air Rings

Linear low density polyethylene (LLDPE) can be drawn down to thin gauges while maintaining superior mechanical properties making these polymers well suited for blown film extrusion. However, because LLDPE polymers have relative low melt strength, dual-orifice (lip) air rings provide improved bubble stability leading to higher DSO with good gauge uniformity.

The design concept of dual-lip air ring is to use a primary or lower lip near the die exit to provide a low volume (high velocity) stream of air and a secondary or upper lip having a diameter 1.2 – 2.5 times the die diameter to provide a large volume of air for cooling (see Figure - 3). The lower and upper lips are separated by a machined conical surface (forming cone), the geometry of the cone establishes the bubble shape and guides the air flow.

The lower lip provides a small volume (high velocity) of air to lock in the bubble and it provides significant cooling of the melt as shown in the calculated heat transfer coefficients along the bubble surface (excluding the heat of crystallization) in Figure - 4. After the forming cone, the bubble is exposed to the upper lip and is cooled by a large volume of air (lower velocity) over a large bubble circumference. Cone angle and height will determine the diameter of the upper lip and thus the minimum blow-up-ratio. The air ring cone can induce significant bubble expansion provided by the force of the Bernoulli Effect. This expansion can significantly reduce residual stress (orientation) in the CD, because stress induced at high melt temperatures will usually relax before they are frozen-in, particularly in polymers with fast relaxation times such as LLDPE and m-LLDPE.

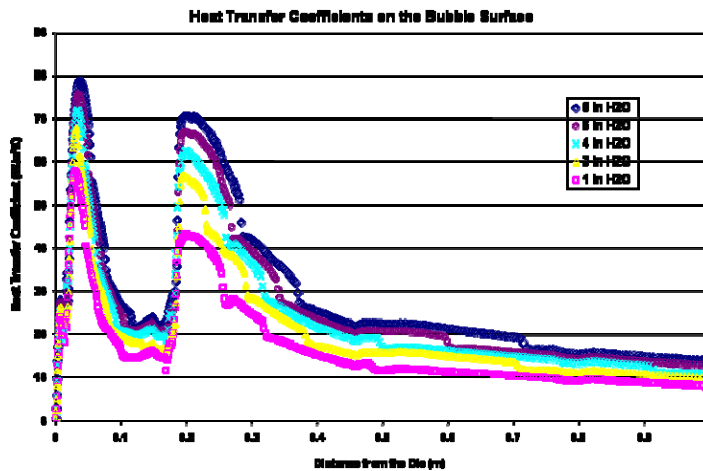


Figure – 4 Calculated heat transfer coefficients on bubble surface at various air ring pressures on a Future Design air ring. (Sidiropoulos and Vlachopoulos)

The bubble surface temperature can be scanned using an IR sensor (3.4  $\mu$  wavelength) designed for measuring polyethylene temperature. A typical bubble temperature profile is shown in Figure - 5. The heat of crystallization of polyethylene is an exothermic reaction (releasing heat as crystallization occurs); therefore the rate of change of temperature of the bubble surface will slow with the release of heat as crystallization continues.

The melt temperature ( $T_m$ ) is measured with a variable depth thermocouple immersed in the middle of the adapter flow. The bubble surface temperature at the exit of the air ring cone is ( $T_{cone}$ ). The detection of the on-set of crystallization is measured by changing of the slope of the cooling curve, and is defined as the crystallization line height (CLH). The frost line height (FLH) is the position on the bubble where expansion ends. The end of the plateau is defined as the plateau line height (PLH). The end of primary crystallization in the bubble occurs at the freeze line height (FZH).

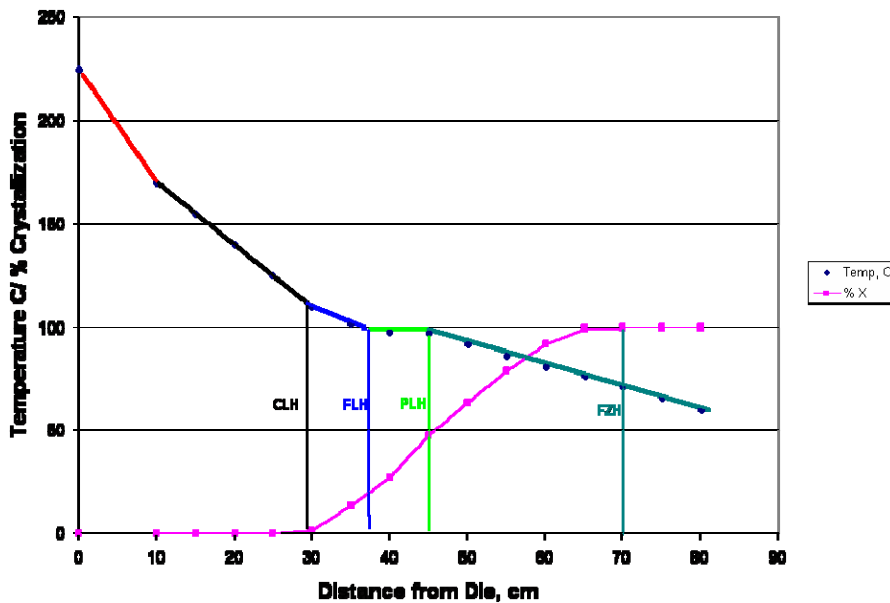
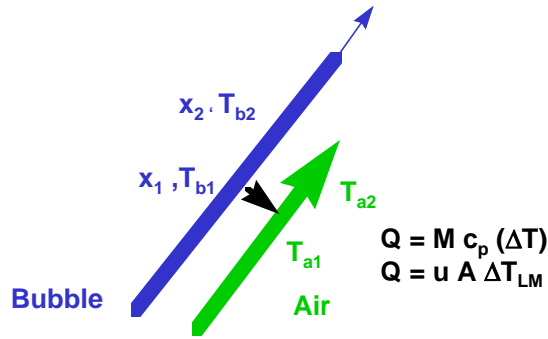


Figure – 5 Bubble temperature profile and crystallization.

The heat transfer between any two points on the bubble surface is shown in Figure - 6.



**Figure – 6 Heat transfer on bubble surface.**

The Equation (8) defines the heat transfer from the bubble surface using an average heat transfer coefficient (U).

$$(8) \quad Q = M C_p \Delta T = U A_s \Delta T_{LMTD}$$

Both the bubble and air flow are free surfaces which interact with each other. The cooling air flow is difficult to measure because air is inducted from the environment and interacts with the quenching process. Figure -7 shows the average heat transfer coefficient determined for various regions (including the heat of crystallization) of a blown film bubble.

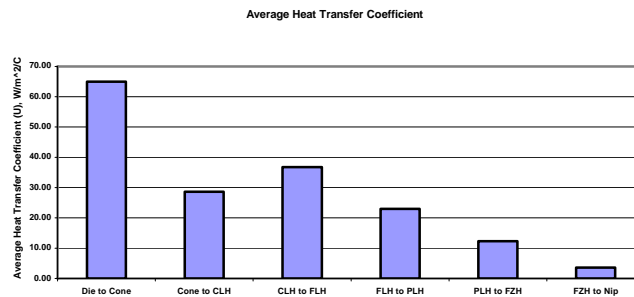


**Figure - 7 Average heat transfer coefficient for various region of the bubble.**

The time that polymer takes to move from the exit of the die to the FLH ( $t_p$ ) depends on the design of the air ring used. For single lip air rings use Equation (9), and for dual lip air rings use Equation (10) can be used for estimates.

(9) Single lip air rings.

$$t_p = [FLH / (V_f - V_o)] * \ln(V_f / V_o) \quad t$$

(10) Dual lip air rings.

$$t_p = [(Cone / (V_c - V_o)) * \ln(V_c / V_o)] + [(FLH - Cone) / (V_f - V_c)] * \ln(V_f / V_c) \quad t$$

The shape of the bubble and the velocity (MD) profile must be determined to calculate the forces being applied to the bubble. Figure – 8 shows the dimensionless MD velocity and bubble radius profile for a blown film bubble.

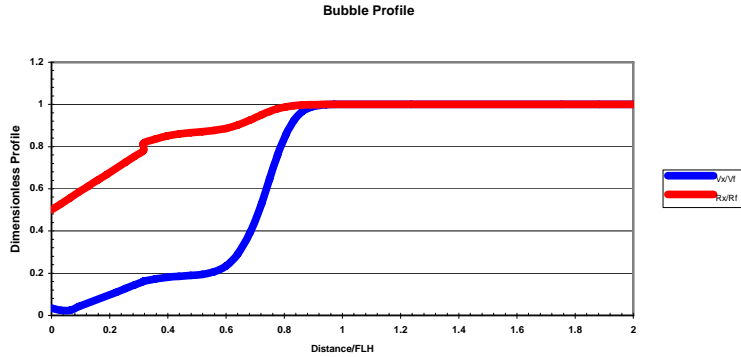


**Figure - 8 MD Velocity and bubble radius profile as a function of distance from the die.**

The analysis of the blown film bubble requires that the stress tensors be developed. To determine the stress tensors the strain rate tensors must first be determined. Figure – 9 shows the strain rates in the MD and CD as a function of distance from the die. The polymer run was a LLDPE (1.0 MI, 0.918 g/cc). The maximum strain rate is sometimes used to describe the strain rate in each direction. However, the extensional flow in both majors axis is not steady-state, but a transient flow. This means that defining the stress built up in the film has to be integrated from the die to the FLH for deformation and relaxation effects.

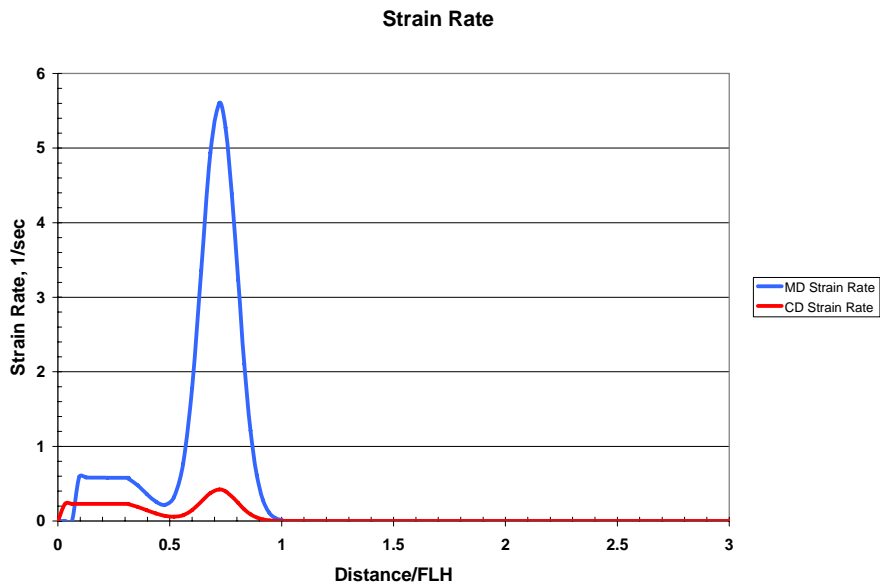


**Figure - 9 Bubble Strain Rates for MD and CD as function of distance from the die.**

Integrating the stress balance in both the MD and CD from the die exit to the FLH will provide the stress “frozen-in” the film as shown in Figure - 10.

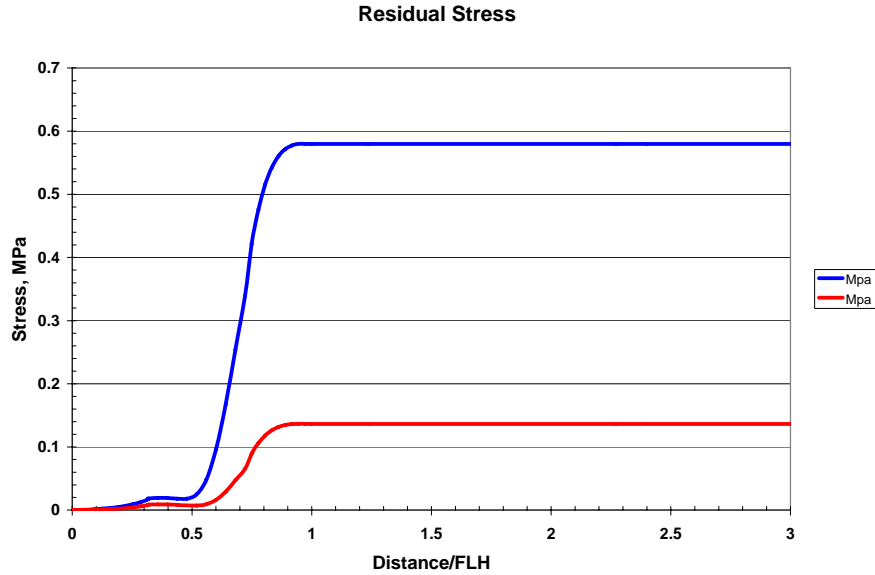


**Figure - 10 Development of MD and CD Residual Stress in Blown Film**

**Orientation/Stress/Forces**

Orientation in a film occurs as the result of stress developed in deformation of the molten polymer fluid combined with stress relaxation until the film is frozen, locking the residual stress into the film's structure. The stress developed is related to the strain rate occurring as the bubble is formed. The calculated stress in the MD is a function of bubble radius and thickness and is calculated using Equation (11).

At x = FLH:

$$(11) \quad \tau_{md} = \frac{F}{(2 \cdot \pi \cdot h_f \cdot r_f)} \quad F/L^2$$

The calculated stress in the circumferential direction (hoop stress) at the FLH is determined using Equation (12).

At x = FLH:

$$(12) \quad \tau_{cd} = \frac{\Delta P \cdot r_f}{h_f} \quad F/L^2$$

Clearly if both the take-up force and internal bubble pressure can be determined, then these equations might be used to predict the forces induced into the film.

**Extensional Viscosity**

There is a significant difference between LLDPE and LDPE polymer flow in extension. Figure – 11 shows the reduced extensional viscosity of a LLDPE (1.0 MI, 0.920 g/cc) compared to a LDPE (1.5 MI, 0.919 g/cc) polymer as a function of zero shear viscosity times strain rate. The LCB of LDPE causes a significant increase in strain hardening in extensional flow which produces a strand rupture (break) at higher strain rates. LLDPE polymers

display a peak viscosity (maximum in the extension viscosity curve) after which draw resonance (DR) begins to occur.

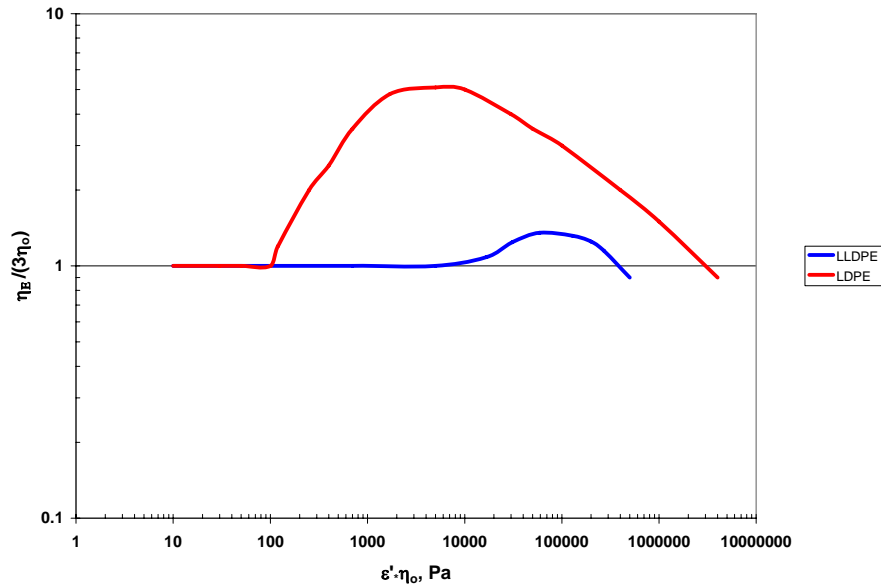


**Figure – 11 Normalized steady-state elongational viscosities for LLDPE (1.0 MI, 0.920 g/cc) and LDPE (1.5 MI, 0.919 g/cc) polymers.**

Extensional viscosity curves have been difficult to develop relationships to actual processes. The problem is that extension is transient in most processes. This means that there is not a unique extensional stress for each strain rate. It is the path that is taken to reach a maximum strain rate that determines the extensional stress and that is unique for each process/polymer system. Another concern for extensional viscosity in blown film is that the extensional process is not iso-thermal. The cooling plays a critical role in the development of stress and in blown film processes.

A method for measuring the apparent extensional viscosity is to continuously draw down a fiber and measure the stress and strain rate using equipment like the Gottfert Rheotens unit shown in Figure – 12.



**Figure – 12 Rheotens melt strength measurement. (Credit: Gottfert)**

The melt strength data for various polymers is shown in Figure – 13. Melt strength is strongly influenced by  $M_w$  as shown with 1.0 MI LDPE vs. the 2.0MI LDPE. Melt strength increases as melt index decreases ( $M_w$  increases).



LCB also increases melt strength as shown by the 1.3 MI POP (w/ LCB) having a similar melt strength to a 1.0 MI LLDPE.

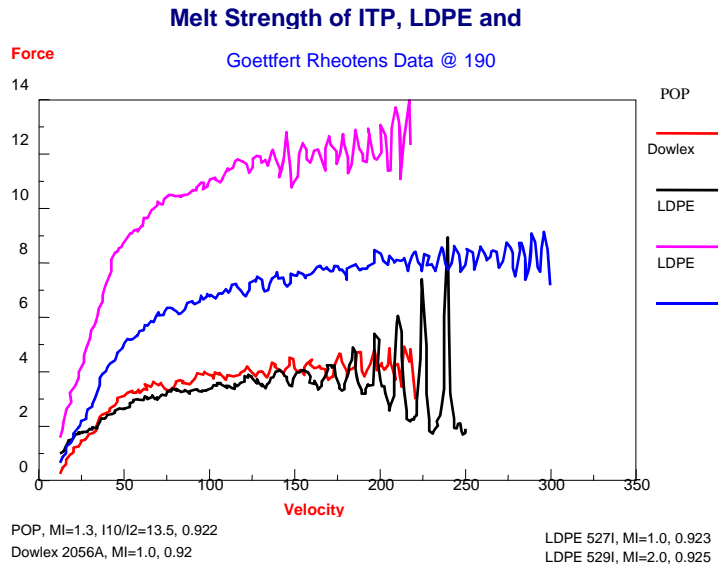


**Figure – 13 Melt strength data for various PE polymers. (Credit: The Dow Chemical Co.)**

The melt strength is determined by measuring the force at a given temperature obtained as the take-off speed is increased Figure – 14 shows the melt strength of a LLDPE (1.0 MI) polymer at 190 °C and  $v_o = 50.8$  mm/sec to be 4.2 cN. There are several methods of running and reporting the melt strength tests:

1. The test can be run at a constant output rate and temperature.
2. The can be run at constant stress on the die and a given temperature.
3. Melt strength can be reported as the maximum force measured as the strand is drawn down.
4. Melt strength is reported as the maximum force obtained with a stable strand.

The method in Figure - 16 reports the maximum force achieved before the strand starts draw resonance running at constant output rate. With some polymers as shown for the LLDPE in Figure – 15, the maximum force can reach quite high values in the unstable region giving possibly misleading test results, if the maximum force is reported. Determining the critical DDR can also be defined as the point of rupture or at the point of on-set of DR. The values from the two results will be different. Using extensional data unless it is known how the values were determined and the conditions of the test could lead to misunderstanding the results as they are applied to other processes.

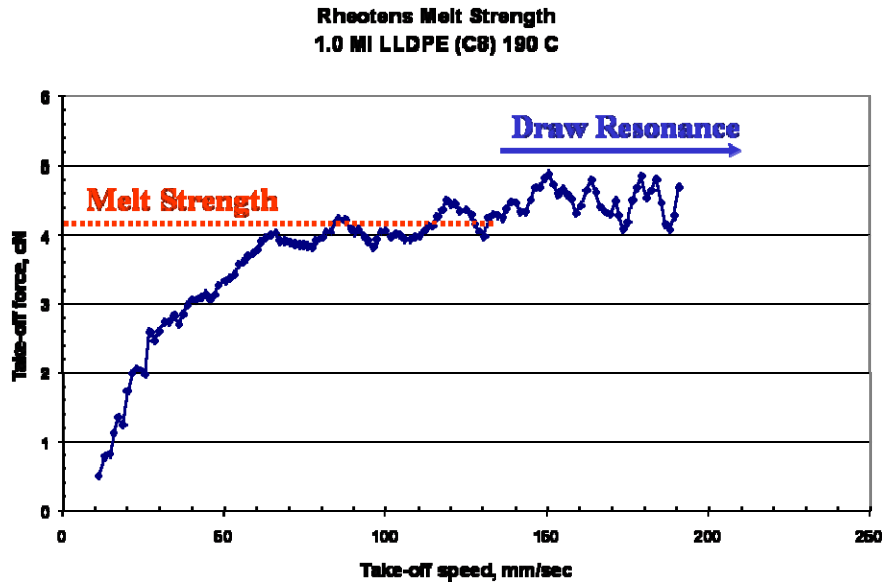


**Figure – 14** Melt strength determination for a LLDPE (1.0 MI, 0.920 g/cc, Z/N C8) run at 190 °C and  $v_0 = 10$  mm/sec. (Credit: The Dow Chemical Co.)

The melt strength test (see Figure – 15) provides a controlled polymer flow (or stress) and temperature to a capillary die (typically 1.0 mm radius). An extruder or a capillary rheometer is used to supply the polymer flow to the die. The extrudate is pulled off the die by a set of either two or four wheels at a determined distance (typically  $H = 100$  mm). The torque on the wheels is recorded as a function of the wheel speed.

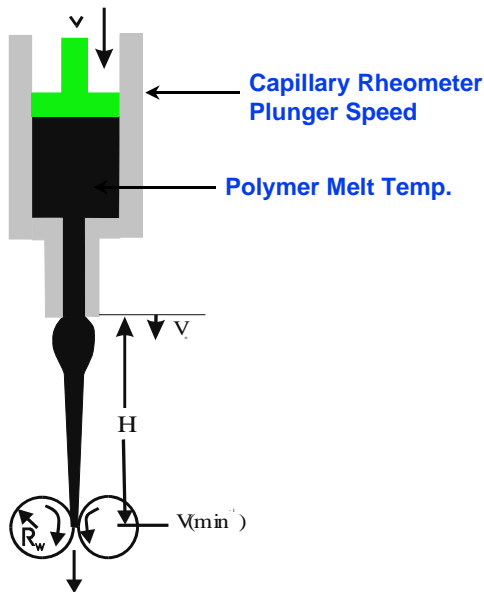


**Figure – 15** Geometry of the melt strength test.

The melt strength data needs to be converted into extensional viscosity data to determine the stress generated in other processes. The strain rate for the melt strength test is determined using Equation (13) developed by Laun. The stress is calculated at the wheels using Equation (14). These equations assume: (1) isothermal conditions, (2) a constant density, (3) a logarithmic velocity function, and (4) a constant output rate. The only assumption that is close to true is the constant output rate. The extensional viscosity model should be non-isothermal, density should be determined as a function of temperature, and a model should be developed based on realistic velocity profiles.

These equations can be used for estimations, but when determining relaxation modulus, better equations need to be developed.

$$(13) \quad \epsilon' = (V_f / H) * \ln (V_f / V_o) \quad 1/t$$

$$(14) \quad \tau_w = (V_f / V_o) * (F / \pi R^2) \quad F/L^2$$

The melt strength of a LLDPE (0.5 MI, 0.918 g/cc, C8) is shown in Figure – 16. The melt strength of 8.0 cN is double the melt strength of the 1.0 MI in Figure – 14. Does higher melt strength mean higher output rates? Usually the higher melt strength allows higher cooling rates to be used, if bubble stability problems are not encountered.

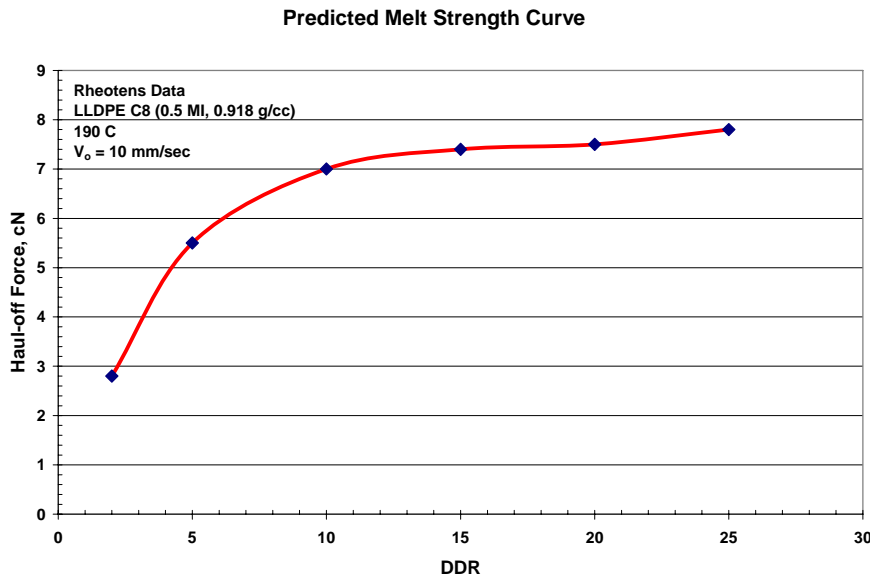


**Figure – 16** Melt strength for 0.5 MI LLDPE run at 190 °C and  $v_o = 10$  mm/sec. (Credit: The Dow Chemical Co.)

**Figure - 17 Relaxation of an initial stress with time.**

The molecules in the bubble are constantly undergoing deformation as well as relaxation from the exit of the die until the FLH. The results of stress balance on a bubble are shown in Figure - 17. Each differential element of film ( $dx$ ) has an initial stress ( $\tau_i$ ) applied to the polymer molecule from the previous element. Added to that is the deformation stress ( $\tau_d$ ) that occurs within the differential element during the time frame ( $dt$ ). The stress remaining after the relaxation of stress that occurs within the time frame ( $dt$ ) results in the residual stress ( $\tau_o$ ) that is passed to the next element as shown with a simple relaxation function in Equation (15).

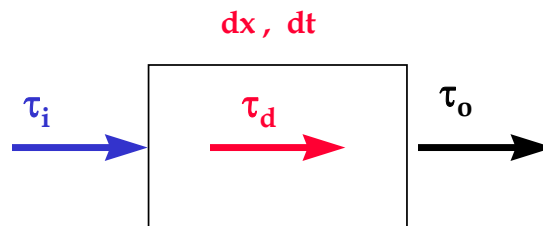


**Figure - 17** Stress balance on a differential element of the polymer in the bubble.

**(15) Relaxation function for predicting stress development.**

$$\tau_o = ((\tau_d + \tau_i) * (1/\exp(\Delta t/\lambda_\epsilon))) \quad t$$

The extensional relaxation time is not the same as the shear relaxation time as characterized by the Cross equation. The analysis of melt strength data revealed that there is not a single relaxation time. The extensional relaxation time ( $\lambda_\epsilon$ ) for a polymer is a function of polymer zero shear viscosity, temperature, strain rate, and the ratio of the process time to the process time at the reference condition as show in Equation (16).

**(16) Extensional relaxation time.**

$$\lambda_\epsilon = \eta_o / (G(\epsilon') * (t_p/t_{p_o})) \quad t$$

The deformational stress ( $\tau_d$ ) is the stress developed during the deformation of the differential element as show in Equation (17).

**(17) Deformational stress**

$$t_d = (3 * \eta_e(\gamma') * \epsilon')$$

Where:  $\gamma' = \epsilon'$

The relaxation modulus for extension is dependent on the strain rate. Figure – 18 shows the relationship of the relaxation modulus (G) as a function of strain rate for LLDPE (0.5 MI, 0.917 g/cc) at 190 °C and a initial velocity  $v_o = 10$  mm/sec using the melt strength test.

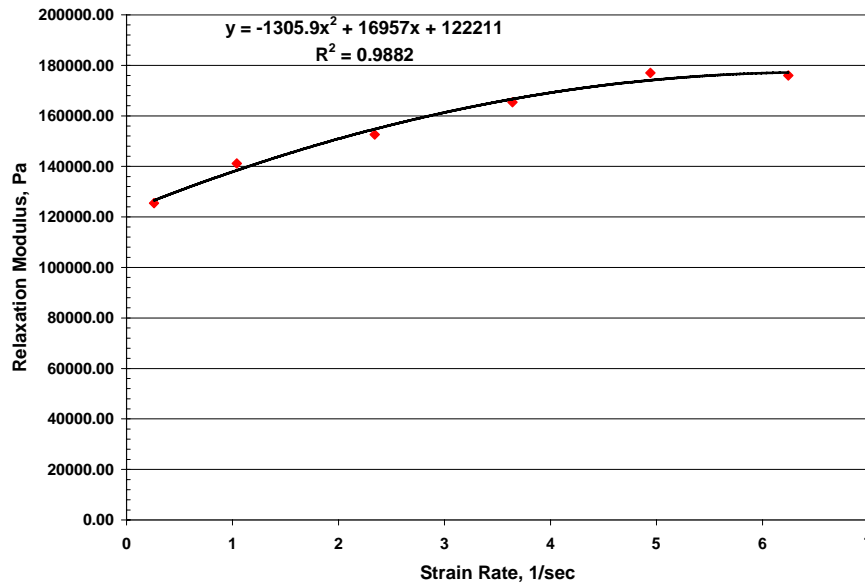


**Figure – 18 Extensional relaxation modulus (G) for LLDPE (0.5 MI, 0.917 g/cc) at 190 °C as a function of maximum strain rate. (Measured using Rheotens test with a  $v_o = 10$  mm/sec.)**

The normalized extensional viscosity of a LLDPE (0.5 MI, 0.917 g/cc) at 190 °C is shown in Figure – 19 at the conditions run in the Rheotens test. The Trouton viscosity is the line  $(3\eta_o) = 1.0$ . This data is indicating that there is a small amount of strain hardening, but certainly not at the levels seen for LDPE. The data is run at 190 °C with a initial velocity of  $v_o = 10$  mm/sec.

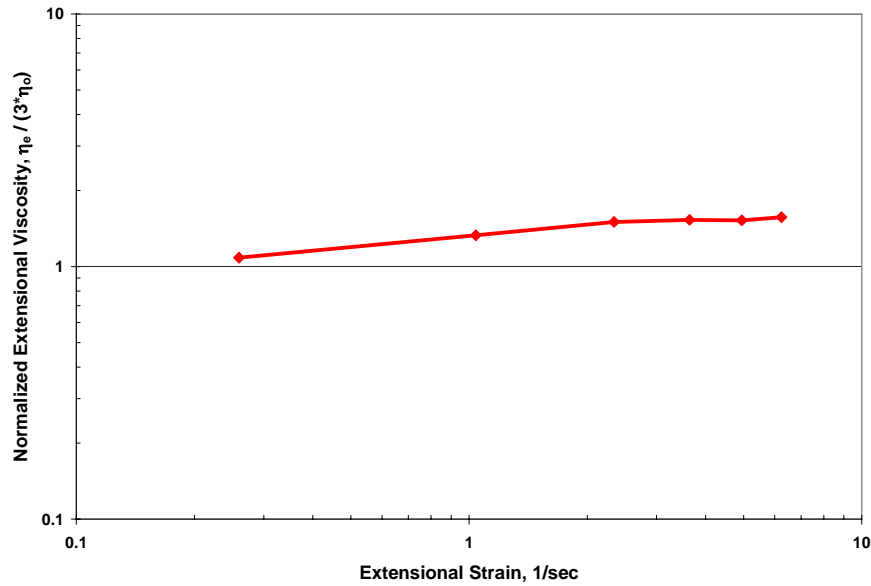


**Figure – 19** Normalized Extensional viscosity for LLDPE (0.5 MI, 0.917 g/cc) at 190 °C and  $v_0 = 10$  mm/sec.

### Orientation

Orientation in a film occurs as the result of stress developed in deformation of the molten polymer fluid combined with stress relaxation until the film is frozen, locking the residual stress into the film's structure. The stress developed is related to the strain rate occurring as the bubble is formed. However, the shape of the bubble can be significantly altered, making these values difficult to predict. Typically a force balance on the bubble surface would be used to determine the residual stress in the MD, CD and ND. The calculated stress in the direction of flow as a function of bubble radius is calculated using Equation (18).

$$(18) \quad \sigma_{11} = \frac{F_L}{(2 \pi r_{fx} h_x)}$$

Where:

$$F_L = \text{take-off force, } F$$

The haul-off force at  $x = FLH$  equation (29) can be rewritten as shown in Equation (19).

$$(19) \quad F_L = \sigma_{11} * (2 \pi r_{fh} h_{fh})$$

The calculated stress in the circumferential direction as a function of distance from the bubble is determined using Equation (20).

$$(20) \quad \Delta P = h * [(\sigma_{11}/R_l) + (\sigma_{33}/R_h)]$$

Where:

$$R_l = \frac{r_f}{\cos \theta} \text{ radius of curvature factor in MD}$$

$$R_h = \frac{-1}{((d^2r/dx^2)\cos^3 \theta)} \text{ radius of curvature factor in CD}$$

The CD or hoop stress at  $x = FLH$ , Equation (19) can be rewritten as Equation (21).

$$(21) \quad \sigma_{33} = \frac{\Delta P r_f}{h_f}$$

The CD force applied from the die to the FLH Equation (20) can be rewritten as shown in Equation (22).

$$(22) \quad F_{CD} = \sigma_{33} * (z_{filh} h_{avg})$$

The calculated stress in the normal direction is determined using Equation (23).

$$(23) \quad \sigma_{22} = \Delta P$$

The normal force applied from the die to the FLH Equation (22) can be rewritten as shown in Equation (24).

$$(24) \quad F_{ND} = \sigma_{22} * (x_{filh} 2 \pi r_{avg})$$

Clearly if the take-up force and internal bubble pressure are known, then these equations might be used to predict the forces applied onto the film. The internal bubble pressure is very easy to measure with a transducer. However, the take-off force is not easily measured on blown film lines.

Orientation in each of the principal directions would be related to the resultant forces applied over the bubble surface in the three principal directions. The magnitude and direction of the resultant force is shown in Equations (25 - 28) and Figure - 20.

$$(25) \quad F_{total} = (F_L^2 + F_H^2 + F_N^2)^{0.5}$$

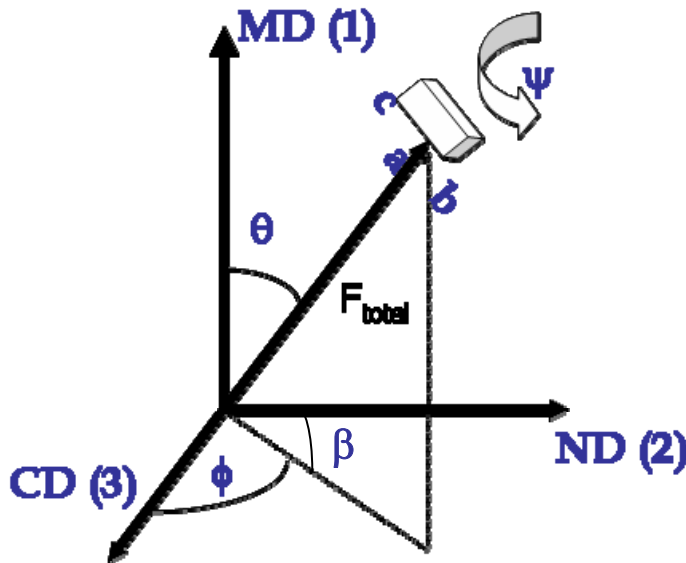


Figure - 20 Development of MD, CD and ND residual forces is directly related to orientation and crystallization of the film.

$$(26) \quad \begin{array}{l} \text{MD force direction angle} \\ \text{Cos}(\theta) \end{array} = (F_L / F_{total})$$

- (27) CD force direction angle  
 $\text{Cos}(\phi) = (F_H / F_{\text{total}})$
- (28) ND force direction angle  
 $\text{Cos}(\beta) = (F_N / F_{\text{total}})$

Figure - 21 shows the relaxation of an initial stress (0.2 MPa) with respect to time using a polymer with a slow extensional relaxation time (1.0 sec), a moderate relaxation time (0.32 sec), and a fast relaxation time (0.032 sec). When the time elements of the blown film process become small enough or the relaxation times become large enough to prevent the stress from relaxing, then increased residual stress will be frozen into the bubble film structure.

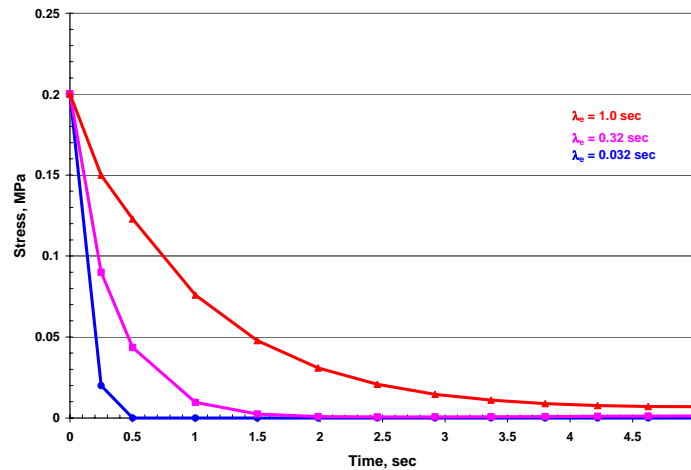


Figure – 21 Relaxation of 0.2 MPa stress using different relaxation times.

Orientation and crystallization influences most film properties. The forces generated during the fabrication of the film will influence the orientation of both the crystalline domains and the tie molecules imbedded in the crystalline structures. These orientations developed have a relationship to the film properties measured on the film.

There were three blown film lines used to collect film samples as shown in Table - I used to collect data. The first line is designated as Line 1. This was a line designed to run LLDPE at high output rates using IBC technology. Line 2 was a general purpose line set up to run LLDPE at moderate rates. Line 3 is a small research line running low rates. The three lines were selected to provide a wide range in process conditions and to include scale-up capability in the model.

**Table – I EXPERIMENTAL EQUIPMENT**

	<u>Line 1</u>	<u>Line 2</u>	<u>Line 3</u>
Extruder	Sterling	Gloucester	Egan
Size, mm	88.9	63.5	50.8
L/D	32	30	24
Drive, Hp	200	100	20
Max. Speed, rpm	105	150	175
Screw	Barr ET	Barr ET	Barrier
Die	Gloucester	Sano	Egan
Die Size, mm	203.2	152.4	76.2
Air Ring:	Saturn-II	Saturn-II	Saturn-II

Blower, Hp	20	7.5	5
IBC	yes	no	no
Winder (max), mpm	244	122	30.5

Polymer used in this study was a Z/N LLDPE octene solution product with a 0.5 dg/min melts index, a 0.918 g/cc density, and an 8 I<sub>10</sub>/I<sub>2</sub> ratio (DOWLEX 2020G LLDPE produced by The Dow Chemical Company).

Film samples (98) were collected at various process conditions shown in Table – II. Seven (7) process parameters were varied and included output rate, die diameter, die gap, melt temperature, film thickness, FLH, and BUR. At each condition data was measured on internal pressure, bubble temperature profile, and bubble radius at the exit of the air ring cone. These results were then used in a blown film process model to determine the critical process characteristics discussed in this paper.

**Table – II Process parameters (Min, Max, and Avg.)**

	Min	Max	Average
<b>Output, kg/hr</b>	12.86235	171.3465	75.85791
<b>Die Diameter, cm</b>	7.62	20.32	15.60286
<b>Die gap, cm</b>	0.1016	0.254	0.180133
<b>Melt Temp, C</b>	218.3333	246.6667	234.0703
<b>Film Thickness, cm</b>	0.00127	0.00762	0.002762
<b>FLH, cm</b>	25.4	114.3	60.46755
<b>BUR</b>	2	3.8	2.527653

The film properties listed in Table -III of each film sample was measured. The blown film process parameters for each run were used in a multivariable model to correlate to the film properties using JMP 6.0 software from SAS.

**Table – III Film property tests.**

Tensiles (MD & CD)	ASTM D-882
Dart Impact (A)	ASTM D-1709
Elmendorf Tear (MD & CD)	ASTM D-1922
PPT Tear (MD & CD)	ASTM D-2582
Gloss (20 & 45)	ASTM D-2457
Haze	ASTM D-1003
Shrinkage (MD)	ASTM D-2732



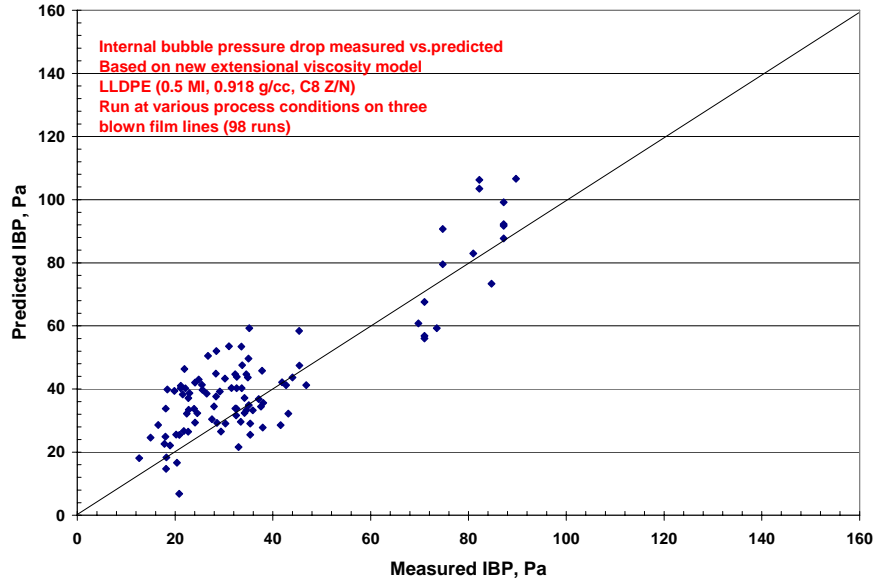
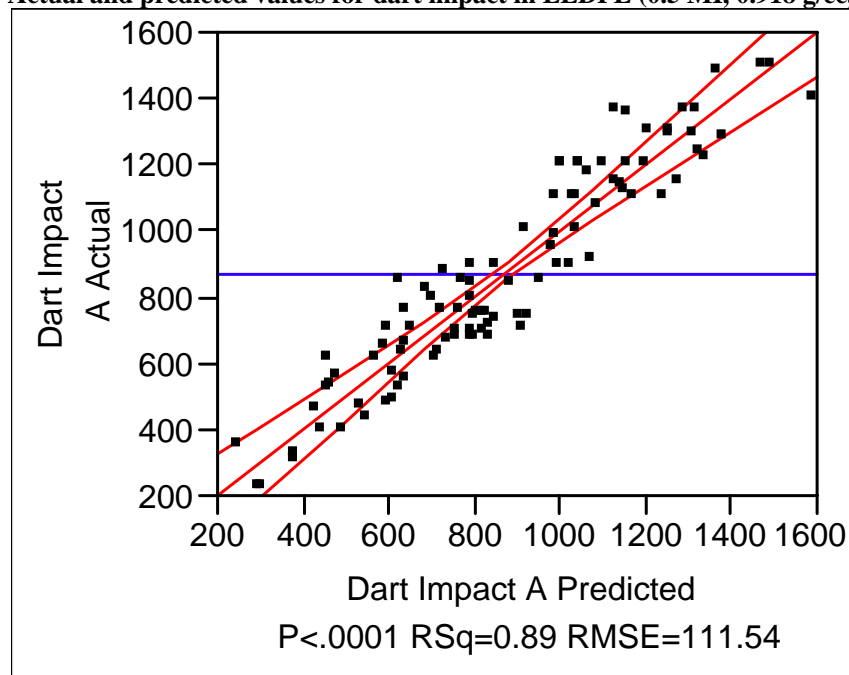


**Figure – 22 Measured and predicted internal bubble pressure for LLDPE (0.5 MI, 0.918 g/cc, C8 Z/N).**

This paper will discuss two film property models obtained with this data, dart impact and MD Elmendorf tear. The first property dart impact actual vs. predicted by the model is shown in Figure – 23. The film sample thickness ranged from 12.7  $\mu$  (0.5 mils) to 76.2 (3 mils). The model correlated fairly well obtaining a  $R^2$  of 0.89. The new extensional viscosity model was used in a blown film model to determine the stress levels developed in the bubble. The only stress level that is easily measured for the blown film process is the internal bubble pressure. Figure – 22 show the results of the measured and predicted internal bubble pressure are actually very similar over a wide range of line size and process conditions.

**Figure – 23 Actual and predicted values for dart impact in LLDPE (0.5 MI, 0.918 g/cc, C8).**



The significant variables for the dart impact model are shown in Table – IV. Significant new discoveries of this model are:

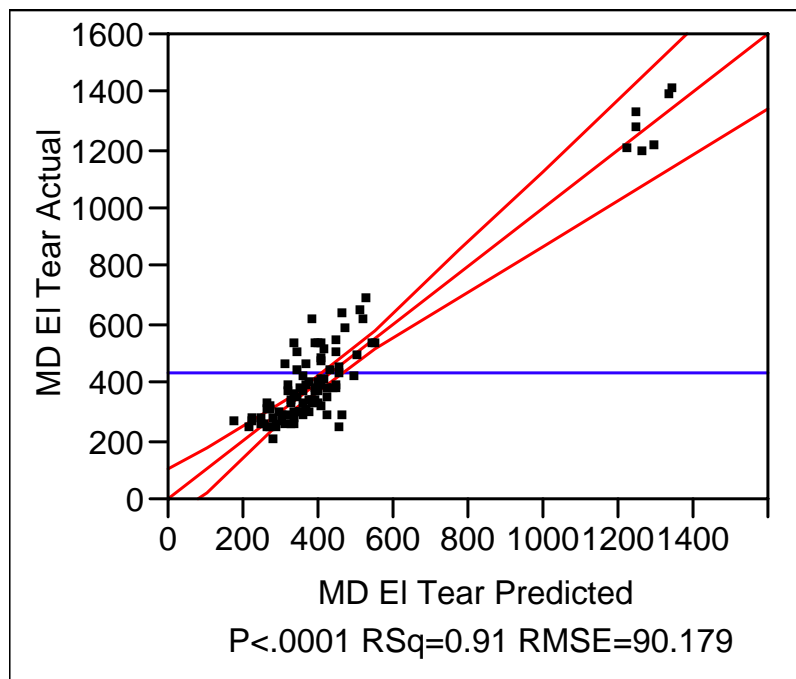
- (1) The influence of the crystallization after the FLH was found to be significant when slow crystallization occurs in this region it reduces dart impact strength as shown with both FZH and PLH-FZH Crystallization Coefficient.
- (2) The residual stresses and forces in both the MD and CD act together to influence dart impact. The force and stress both relate to the orientation induced into the film.
- (3) The faster cooling from the die to the FLH was shown to improve dart impact strength.

**Table – IV Parameter Estimates for Dart Impact (A)**

Term	Estimate	Std Error	t Ratio	Prob> t
Intercept	-1338.521	489.423	-2.73	0.0076
Film Thickness, cm	44960.201	12769.28	3.52	0.0007
BUR	1603.7219	317.7826	5.05	<.0001
DDR	-11.83128	2.70951	-4.37	<.0001
Die ^2	2.6755848	0.299141	8.94	<.0001
FLH^2	-0.07506	0.020308	-3.70	0.0004
BUR^2	-240.5688	60.57947	-3.97	0.0002
FZH, cm	-0.628738	1.418582	-0.44	0.6587
MD Residual Stress, MPa	89.31756	103.1488	0.87	0.3890
CD Residual Stress, MPa	-358.4828	189.5827	-1.89	0.0621
Die - FLH Heat Transf. Coef. U, W/m^2/K	11.777468	1.8648	6.32	<.0001
PLH - FZH Crystallization Coef., W/m^2/K	-60.41775	9.048179	-6.68	<.0001
Fmd, N	-20.63644	2.570375	-8.03	<.0001
Fcd, N	2.7622835	1.018136	2.71	0.0081

Figure – 24 shows the model actual and predicted results for MD Elmendorf tear strength for the film samples. The model had a good  $R^2$  of 0.91.

**Figure – 24 Actual and predicted values for MD Elmendorf tear in LLDPE (0.5 MI, 0.918 g/cc, C8).**



The significant variables for the MD Elmendorf tear model are shown in Table – V. Significant new discoveries of this model are:

- (1) Faster cooling improves MD Tear as shown by FLH and die to FLH heat transfer coefficient and aspect ratio.
- (2) CD orientation also improves MD tear as shown by CD force, MD direction angle and ND direction angle, and CD We number results.
- (3) The complex nature of MD Elmendorf tear is also shown with interactions of die gap-BUR, die gap-DDR and die gap-output rate.

**Table – V Parameter Estimates for MD Elmendorf Tear**

Term	Estimate	Std Error	t Ratio	Prob> t
Intercept	1676.2098	721.1042	2.32	0.0228
Output, kg/hr	9.0325842	3.911603	2.31	0.0237
Die gap, cm	160.82236	555.6716	0.29	0.7731
Melt Temp, C	-4.239417	2.014232	-2.10	0.0387
Film Thickness, cm	172963.71	16830.48	10.28	<.0001
FLH, cm	-12.55273	8.536955	-1.47	0.1456
BUR	19.06761	83.57186	0.23	0.8201
DDR	3.215412	2.504181	1.28	0.2031
Out ^2	-0.026423	0.014672	-1.80	0.0757
Die ^2	0.8650403	0.510484	1.69	0.0943
FLH^2	0.0367404	0.044839	0.82	0.4152
cone diameter, cm	-8.417692	7.524361	-1.12	0.2668
Aspect Ratio ( FLH / r <sub>o</sub> )	-4.870285	33.31222	-0.15	0.8842
Nusselt ( U D / k )	-79442.6	37580.69	-2.11	0.0378
Weissenberg CD ( $\lambda * \epsilon'$ )	-4.169396	261.8218	-0.02	0.9873
Die - FLH Heat Transf. Coef. U, W/m^2/K	8.6506514	5.403724	1.60	0.1136
Internal Bubble Pressure, Pa	-4.219556	1.665719	-2.53	0.0134
Fcd, N	3.6715164	1.905032	1.93	0.0577
MD direction angle	-1.346336	2.027445	-0.66	0.5087
ND direction angle	-5.924511	2.802269	-2.11	0.0378
(Die gap, cm-0.18013)*(BUR-2.52765)	-3054.883	1263.713	-2.42	0.0181
(Die gap, cm-0.18013)*(DDR-24.5488)	-132.5648	40.23502	-3.29	0.0015
(Output, kg/hr-75.8579)*(Die gap, cm-0.18013)	0.502397	12.24316	0.04	0.9674

## Summary

The prediction of film properties based on polymer properties and processing conditions has been a goal for many years. There are several new developments discussed in this paper. The development of a new extensional viscosity model to allowed accurate prediction of the stress on the bubble surface. The new model is based on development on a novel relationship between strain rate and the polymer relaxation time.

The new model is much more accurate in predicting the stresses based on polymer parameters and processing conditions without the need for any adjusting factors. The new model will also predict the different forces measured with different processing conditions using the melt strength test using the same polymer parameter.

The determination of stresses on the bubble allows the calculation of the magnitude and direction of the resultant force vector. The model also calculates the cooling and crystallization kinetics. The determination of these critical process parameters were used to develop fairly simple multivariable regression models to predict very complex film properties such as dart impact strength and MD Elmendorf tear properties based on processing conditions.

The results of the film property modeling have confirmed that there is a relation between orientation and quenching rates on film properties. Knowledge of the forces on the bubble and the rate of cooling were identified as having significant influence on film properties.

Terms used in this paper:

A	=	Aspect Ratio	
$A_s$	=	Surface area,	$L^2$
$a_T$	=	Temperature shift factor	
BUR	=	Blow Up Ratio	
Cone	=	Cone height,	L
$C_p$	=	Heat capacity,	$H/(M^*T)$
D	=	Diameter of die annulus	L
DDR	=	Draw Down Ratio	
De	=	Deborah number	
$E_a$	=	Activation Energy	
F	=	Haul-off force	F
FLH	=	Frost Line Height,	L
G	=	Extensional relaxation modulus	$F/L^2$
H	=	Distance between die and haul-off wheels	L
$H_f$	=	Heat of fusion,	H/M
$h_f$	=	Final film thickness	L
M	=	Mass flow rate	M/t
n	=	Power law exponent	
Q	=	Heat transferred,	H/t
R	=	Gas Constant	
$r_f$	=	Final radius of bubble	L
$r_o$	=	Radius of die	L
T	=	Temperature,	T
t	=	Time	t
$T_o$	=	Reference temperature (normally $190\text{ }^\circ\text{C} = 463.15\text{ }^\circ\text{K}$ )	T
$t_p$	=	Characteristic process time,	t
U	=	Local heat transfer coefficient	$H/(t^*L^2*T)$
V	=	Velocity	L/t
X	=	Fraction crystallinity,	
z	=	Distance from die on bubble surface,	L
$\Delta p$	=	Internal bubble pressure	$F/L^2$
$\Delta t$	=	Time interval of element	t
$\epsilon'$	=	Strain rate,	1/t
$\gamma'$	=	Shear rate,	1/t
$\eta$	=	Shear viscosity,	$M/(L\ t)$
$\eta_e$	=	Extensional viscosity,	$M/(L\ t)$
$\eta_o$	=	Zero shear viscosity,	$M/(L\ t)$
$\lambda_s$	=	Shear relaxation time,	t
$\lambda_e$	=	Extensional relaxation time,	t
$\rho_s$	=	Density, solid	$M/L^3$
$\tau$	=	Stress,	$F/L^2$


## REFERENCES

1. Huck, N. D., and Clegg, P. L., "The Effect of Extrusion Variables on the Fundamental Properties of Tubular Polyethylene Film", SPE ANTEC 1961, 18-2 pages 1-14.
2. J. Audureau, BB. Morese-Seguela, D. Constantin, and O. Gode, "Prediction and Improvement of Surface Properties of Tubular Low Density Polyethylene Films", Journal of Plastic Film & Sheeting, Vol. 2, page 298, October, 1986.
3. N. Billon, P. Barq, and J. M. Haudin, "Modeling of the Cooling of Semi-crystalline Polymers during Their Processing", International Polymer Processing VI, Vol. 4, page 348, 1991.

4. T. I. Butler and R. Patel, "Blown Film Bubble Forming and Quenching Effects on Film Properties", TAPPI PL&C, page 409, 1992.
5. John Dealy and Kurt Wissbrun, "Melt Rheology and Its Role in Plastics Processing", Van Nostrand Reinhold, New York.
6. Robert Farber and John Dealy, "Strain History of the Melt in Film Blowing", Polymer Engineering and Science, Vol. 14, No. 6, page 435, June, 1974.
7. C. D. Han and T. H. Kwack, "Rheology-Processing-Property Relationships in Tubular Blown Film Extrusion. II. High Pressure Low-Density Polyethylene", Journal Of Applied Polymer Science, Vol. 28, page 3399, 1983.
8. T. A. Huang and G. A. Campbell, "Deformational History of LLDPE/LDPE Blends on Blown Film Equipment", Advances in Polymer Technology, Vol. 5, No. 3, page 181.
9. T. Kanai and J. L. White, "Kinematics, Dynamics and Stability of the Tubular Film Extrusion of Various Polyethylenes", Polymer and Textile Research Association, University of Tennessee, Knoxville, PATRA Report No. 203, April, 1983.
10. T. Nagasawa, T. Matsumura, S. Hoshino, and K. Kobayashi, "Film Forming Process of Crystalline Polymer. I. Factors Inducing A Molecular Orientation in Tubular Blown Film", Applied Polymer Symposium, No. 20 page 275, 1973.
11. G. Panagopoulos and L. G. Hazlitt, "Next Generation High Performance LLDPE Blown Film Resins: Superior Physical Properties and Processability", SPE Polyolefin ANTEC, page 266, 1993.
12. J. R. A. Pearson and C. J. S. Petrie, "The Flow of a Tubular Film. Part 1. Formal Mathematical Representation", Journal of Fluid Mechanics, Vol. 40, page 1, 1970.
13. J. R. A. Pearson and C. J. S. Petrie, "The Flow of a Tubular Film. Part 2. Interpretation of the Model and Discussion of Solutions", Journal of Fluid Mechanics, Vol. 42, page 609, 1970.
14. D. Simpson and I. Harrison, "The Use of Deformation Rates in the Scale-up of Polyethylene Blown Film Extrusion", Journal of Plastic Film & Sheeting, Vol. 8, page 192, July, 1992.
15. P. A. Sweeney, G. A. Campbell, and F. A. Feeney, "Real Time Video Techniques in the Analysis of Blown Film Instability", International Polymer Processing VII, Vol. 3, page 229, 1992.
16. T. Kanai, M. Kimura, and Y. Asano, "Studies on Scale-Up of Tubular Film Extrusion", SPE ANTEC, page 912, 1986.
17. S. M. Alaie and T. C. Papanastasiou, "Modeling of Non-isothermal Film Blowing with Integral Constitutive Equations", International Polymer Processing, Vol. VIII, Issue 1, page 51, March, 1993.
18. T. I. Butler, S. Y. Lai, and R. Patel, "Scale-up Factors Effecting Crystallization In Polyolefin Blown Film", TAPPI PL&C Conference, page 289, 1994.
19. Paul Tas, "Film Blowing- From Polymer to Product", Phd. Thesis Technical University Eindhoven, October 28, 1994.
20. Knittel, R.R. and DeJonghe, R.J. Jr., "Blown Film Cooling Systems," 1992 Film Extrusion Manual, TAPPI PRESS, Atlanta, p. 261.
21. Butler, T.I., "Blown Film Bubble Instability Induced by Fabrication Conditions," 1999 Polymers, Laminations and Coating Conference Proceedings, TAPPI PRESS, Atlanta, p. 815.
22. Sidiropoulos, V and Vlachopoulos J., "An Investigation of Venturi And Coanda Effects In Blown Film Cooling" International Polymer Processing, in Press 1999.
23. Bode, W.W., "Current Developments in Equipment for Processing High Molecular Weight High Density Polyethylene Film," 1989 Polymers, Laminations and Coating, A TAPPI PRESS Anthology of Published Papers 1986-1991, Ed., Bentley D.J. Jr., TAPPI PRESS Atlanta, p. 312.
24. Perdikoulis, J and Smith D., "Evaluation of the Performance of a New Tandem Air Ring System," 1991 Polymers, Laminations and Coating, A TAPPI PRESS Anthology of Published Papers 1986 - 1991, Ed., Bentley D.J. Jr., TAPPI PRESS, Atlanta, p. 324.
25. Stobie, J., "Air Ring Considerations For Optimizing Blown Film Properties," 1996 Polymers, Laminations and Coating Conference Proceedings, TAPPI PRESS, Atlanta, p. 231.
26. Jones, D.N., "USC-1 New Cooling System for LLDPE," 1984 Polymers, Laminations and Coating Conference Proceedings, TAPPI PRESS, Atlanta, p. 105.
27. Gregory, R.B., "Internal Air Ring for Blown Film," 1974 Paper Synthetics Conference Proceedings, TAPPI PRESS, Atlanta, p. 263.
28. DeJonghe, R.J. Jr., "Thermal Analysis of Blown Film Quenching," 1986 Coextrusion Conference Proceedings, TAPPI PRESS, Atlanta, p. 67.

29. Planeta, M., "Test Developments in Blown Film Cooling," 1983 Paper Synthetics Conference Proceedings, TAPPI PRESS, Atlanta, p. 359.
30. Paulius, J., "Water Quenching of Blown Film," 1985 Polymers, Laminations and Coating Conference Proceedings, TAPPI PRESS, Atlanta, p. 197.
31. Silagy, D, J. Non-Newtonian Fluid Mech., "Stationary and Stability Analysis of the Film Casting Process", page 563-583, vol. 79 (1998).
32. Silagy, D., "A Theoretical & Experimental Analysis of Line Speed Limitations in the Film Casting of Polyethylene", 6th European TAPPI Seminar on Polymers, Films, and Coatings, Copenhagen, June 8-9, 1999.
33. Denn, M., "Instabilities in Polymer Processing", AICHE J., (22), No. 2, p 209 - 236, (March, 1976).
34. Anturkar, N., "Draw Resonance Film Casting of Viscoelastic Fluids: a Linear Stability Analysis", J. of Non-Newtonian Fluid Mech., 28, p 287-307, (1998).
35. Pis-Lopez, M., Multilayer Film Casting of Modified Giesekus Fluids Part 1. Steady State analysis", J. Non-Newtonian Fluid Mech., 66 p 71 – 93, (1996).
36. Bortner, M., "Dependence of Draw Resonance on Extensional Rheological Properties of LLDPE", SPE 2003 ANTEC.
37. Smith, Spencer, "Numerical Simulation of Film Casting Using an Updated Lagrangian Finite Element Algorithm", Polymer Engineering and Science, May 2003, Vol. 43, No. 5, page 1105.

www.placecon.org



**2006 PLACE Conference**  
**September 17-21**  
**Cincinnati, Ohio**

**Predicting Blown Film Residual Stress Levels**  
**Influence on Properties**

Presented by:  
**Thomas I. Butler**  
 Owner  
**Blown Film Technology, LLC**

1

---

---

---

---

---

---

---

---

**Introduction**

- Polyethylene film properties are strongly affected by polymer design and processing conditions.
- Polymer design parameters that affect film properties include Density, Mw and MWD, branching and branching distribution.
  - Extensional viscosity model developed to predict bubble stresses.
  - Crystallization model developed to characterize quenching.
  - Air ring design and operation was included in model.
  - Film property differences are the result of processing conditions which produce changes in molecular orientation and crystallization.

2

---

---

---

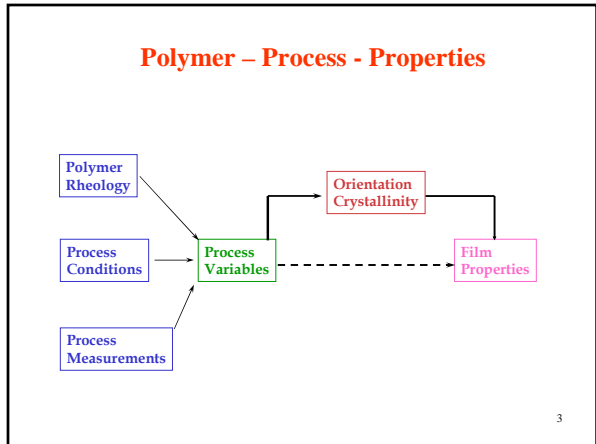
---

---

---

---

---




---

---

---

---

---

---

---

---

### Blown Film Process Variables

**Legend:**

- $h$  = thickness
- $R$  = radius
- $T$  = temperature
- $\rho$  = density
- $z$  = distance from die
- $t$  = time
- $\Delta P$  = bubble pressure
- $F$  = Haul-off force
- $Q$  = output rate
- $V$  = velocity
- $H$  = Heat load
- $U$  = overall heat transfer coeff.
- $c_p$  = heat capacity
- $H_f$  = heat of fusion

\* No air ring  
\* No crystallization model

4

---

---

---

---

---

---

---

---

---

---

---

---

### Characteristic Bubble Angle

**Characteristic bubble angle ( $\alpha_b$ )**

$$\alpha_b = \text{atan}((R_f - R_d) / x_{nh})$$

$R_d = 4\text{-inch}$   
 $R_f = 10\text{-inch}$   
 $BUR = 2.5$   
 $x_{nh} = 25\text{-inch}$

$$\alpha_b = \text{atan}((10-4)/25) = 13.49^\circ$$

5

---

---

---

---

---

---

---

---

---

---

---

---

### Air Ring Design

**The upper lip ( $R_c$ ) has a larger diameter than the lower lip ( $R_d$ ).**  
 $R_c / R_d = 1.2 - 2.0$

**The angle ( $\alpha_c$ ) of the air ring cone**

$$\alpha_c = \text{atan}((R_c - R_d) / x_c) = \text{atan}((6.5-4)/9.5) = 14.75^\circ$$

**The chimney angle ( $\alpha_{chim}$ )**

$$\alpha_{chim} = \text{atan}((R_{chim} - R_d) / x_{chim}) = \text{atan}((8-4)/14) = 15.94^\circ$$

$R_c / R_d = 6.5/4 = 1.625$

6

---

---

---

---

---

---

---

---

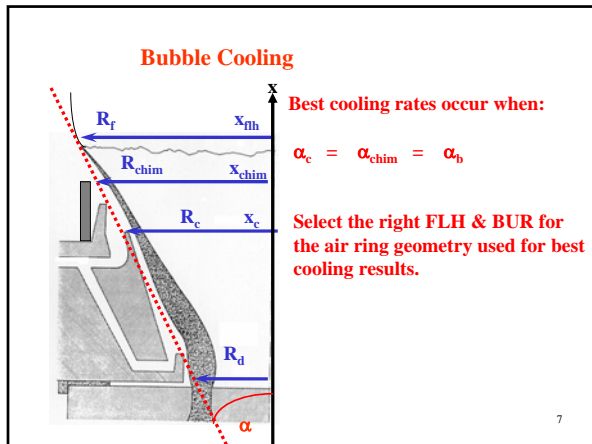
---

---

---

---






---

---

---

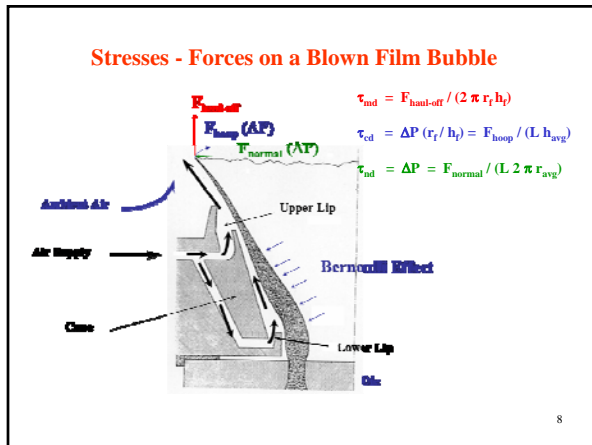
---

---

---

---

---




---

---

---

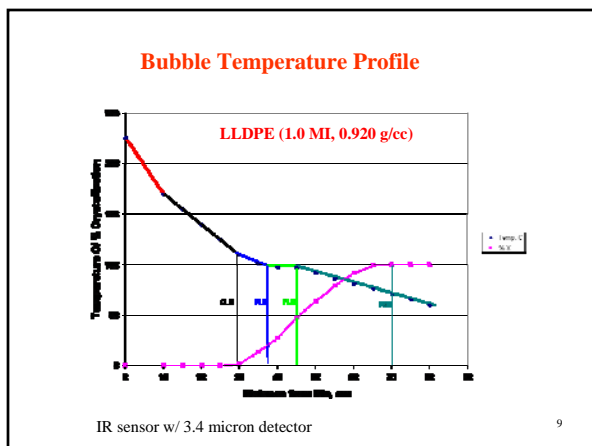
---

---

---

---

---




---

---

---

---

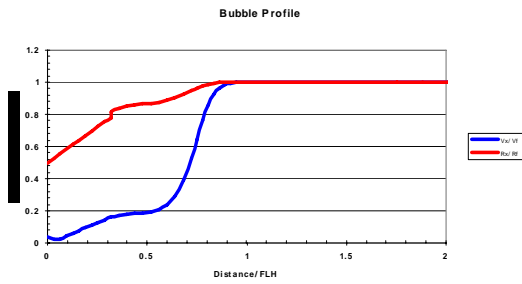
---

---

---

---

### Bubble Radius and Velocity



10

---

---

---

---

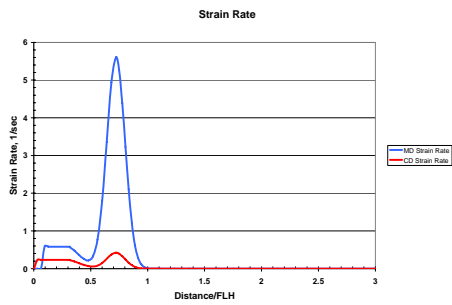
---

---

---

---

### Bubble Strain Rate MD & CD



11

---

---

---

---

---

---

---

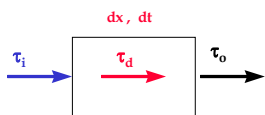
---

### Extensional Viscosity Model

$$\tau_d = (3 * \eta(\dot{\gamma}) * \dot{\epsilon}') \quad (\dot{\gamma}' = \dot{\epsilon}')$$

$$\tau_o = (\tau_d + \tau_i) * (1/\exp(\Delta t/\lambda_e))$$

$$\lambda_e = \eta_o / G(\dot{\epsilon}', t_p/t_{p_o})$$



12

---

---

---

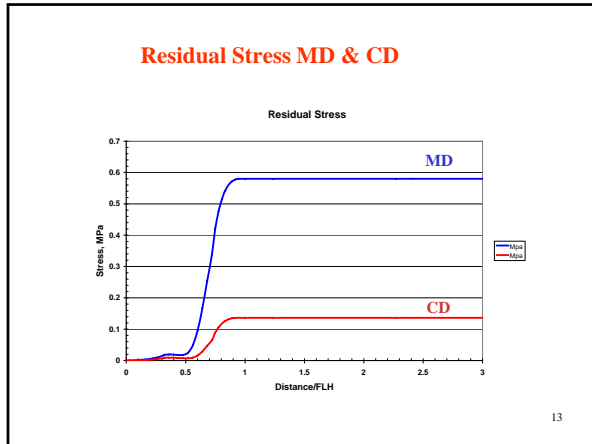
---

---

---

---

---




---

---

---

---

---

---

---

---

---

---

- ### Forces Vectors on Bubble
- Forces acting on Bubble
    - MD Force
      - $F_{\text{haul-off}} = \tau_{\text{md@FLH}} * (2 * \pi * r_f * h_f)$
    - CD Force
      - $F_{\text{hoop}} = \Delta P * (r_f / h_f) * (h_{\text{avg}} * z_{\text{filh}})$
    - ND Force
      - $F_{\text{normal}} = \Delta P * (2 * \pi * r_{\text{avg}} * x_{\text{filh}})$
  - Force  $\cong$  Degree of orientation  
 $\cong$  Degree of bubble stability
- 14

---

---

---

---

---

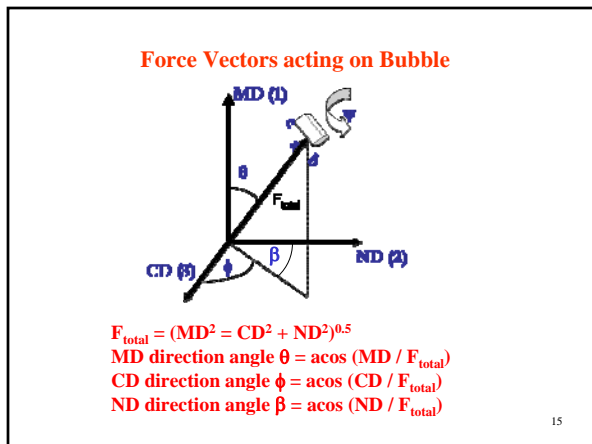
---

---

---

---

---




---

---

---

---

---

---

---

---

---

---

### Force Vectors

LLDPE C8 (1.0 dg/min, 0.920)  
2.5 BUR, 28 inch FLH, 250 lb/hr  
8-inch die, 420 F

F <sub>nd</sub> , Lb <sub>f</sub> (N)	3.62	16.08
F <sub>cd</sub> , Lb <sub>f</sub> (N)	0.42	1.87
F <sub>nd</sub> , Lb <sub>f</sub> (N)	3.44	15.30
Force Vector, psi (N)	5.01	22.27
Force Vector MD angle	6.62	8.62
Force Vector CD angle	46.43	46.43
Force Vector ND angle	83.05	83.05

16

---

---

---

---

---

---

---

---

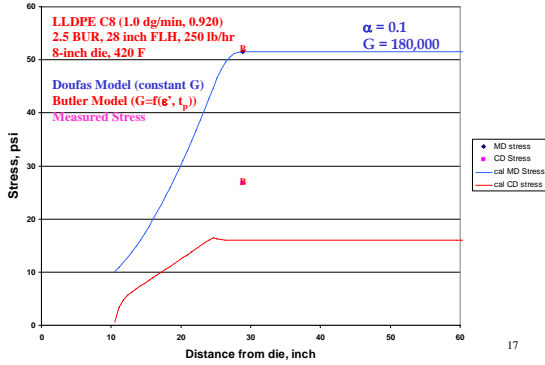
---

---

---

---

### Prediction vs. Measured Stress



17

---

---

---

---

---

---

---

---

---

---

---

---

### Other Critical Process Parameters

- $Q = M C_p \Delta T = U A_x \Delta T_{LMTD}$
- $(H_f \rho 2 \pi r_x h_x V_z \Delta X) / D_z = -C (T_x - T_a) 2 \pi r_x$
- $X' = \Delta X / \Delta t$
- $Nu = U D / k$
- $De = \lambda_c * (V_o / FLH)$
- $A = FLH / r_o$
- $\lambda_c = \eta_o / G(\epsilon', t_p / t_{p,o})$

18

---

---

---

---

---

---

---

---

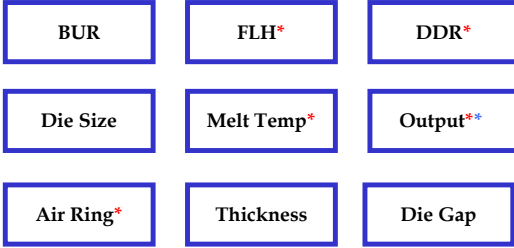
---

---

---

---

### 9 Primary Variables



\* Not Independent Variables  
 \* Output is only time sensitive variable

19

---

---

---

---

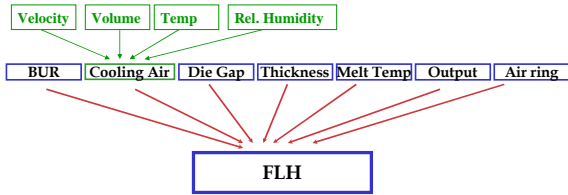
---

---

---

---

### FLH Interactions



20

---

---

---

---

---

---

---

---

### LLDPE Polymer

- Melt Index            0.5            dg/min
- Density                0.918        g/cc
- LLDPE                Z-N        catalyst
- Process                Solution
- Comonomer            Octene
- I10/I2                 8.0
- Slip                    900        ppm
- A/B                    5000       ppm
- PPA                    800        ppm

21

---

---

---

---

---

---

---

---

### Study: 3 - Blown Film Lines

	<u>Line 1</u>	<u>Line 2</u>	<u>Line 3</u>
Extruder	Sterling	Gloucester	Egan
Size, mm	88.9	63.5	50.8
L/D	32	30	24
Drive, Hp	200	100	20
Max. Speed, rpm	105	150	175
Screw	Barr ET	Barr ET	Barrier
Die	Gloucester	Sano	Egan
Die Size, mm	203.2	152.4	76.2
Air Ring:	Saturn-II	Saturn-II	Saturn-II
Blower, Hp	20	7.5	5
IBC	yes	no	no
Winder (max), mpm	244	122	30.5

Credit: The Dow Chemical Company

22

### (7) Process Parameters

	<u>Min</u>	<u>Max</u>	<u>Average</u>
Output, kg/hr	12.86	171.34	75.85
Die Diameter, cm	7.62	20.32	15.60
Die gap, cm	0.1016	0.254	0.1801
Melt Temp, C	218.3	246.7	234.1
Film Thickness, cm	0.00127	0.00762	0.002762
FLH, cm	25.4	114.3	60.5
BUR	2	3.8	2.53

98 Film samples were fabricated

Polymer used:

LLDPE Z/N C8 Solution

1.0 MI, 0.918 g/cc, 8 I<sub>10</sub>/I<sub>2</sub>

S, A/B, PPA, A/O (1<sup>st</sup> & 2<sup>nd</sup>)

23

### (19) Input Parameters for New Model

	<u>Eng.</u>	<u>SI</u>
Output, lb/hr (kg/hr)	250	114
Die Diameter, inch (cm)	8	20.32
Die gap, mils (cm)	100	0.254
Melt Temp, F (C)	450	232.22
Film Thickness, mil (cm)	1	0.00254
FLH, in (cm)	30	76.2
BUR	2.5	2.50
Air Ring Head Pressure, inch of H <sub>2</sub> O, (Pa)	6	1494
Xtal. Temp, F (C)	209.29	98.49
Temp at nip roll, F (C)	100.00	37.78
Nip roll height, in (cm)	240.00	609.60
Temp at FZH, F (C)	158.00	70.00
Temp at CLH, F (C)	230.00	110.00
Air ring, height, inch (cm)	9.5	24.13
Air ring upper cone diameter, inch (cm)	14	35.56
CLH, in (cm)	22.00	55.88
PLH, in (cm)	33.20	84.33
FZH, in (cm)	69.00	175.26
Temp at cone, F (C)	310	154.44

### Calculated Parameters

DDR	32.61	32.61
Shear rate (sec-1)	61	61
Sp Output, lb/hr/in-c (kg/hr/mm-d)	9.95	0.56
Melt Velocity, fpm (cm/sec)	5.12	2.60
Melt Density, lb/ft <sup>3</sup> (g/cc)	46.73	0.7485
MD Strain rate, (sec-1)	5.89	5.89
CD Strain rate, (sec-1)	0.76	0.76
Process Time to FLH, sec	5.94	5.94
Shear Stress, psi (MPa)	18.98	3.171
MD Residual Stress, psi (MPa)	104.07	0.718
CD Residual Stress, psi (MPa)	37.20	0.257
Polymer Extensional Relaxation Time at CLH, sec	0.1999	0.1999
Aspect Ratio ( FLH / r <sub>e</sub> )	7.50	7.50
Reynolds (ρ D Vo / η )	0.0018	0.0018
Deborah ( λ * (Vo/FLH) )	0.0068	0.0068
Nusselt ( U D / k )	0.0085	0.0085
Weissenberg MD ( λ * e' )	1.1779	1.1779
Weissenberg CD ( λ * e' )	0.1517	0.1517
Die - FLH Heat Transf. Coef. U, Btu/hr/in <sup>2</sup> /F (W/m <sup>2</sup> /K)	0.1629	41.10

25

### Calculated Parameters (cont'd)

CLH - FLH Crystallization Coef., Btu/hr/in <sup>2</sup> /F (W/m <sup>2</sup> /K)	0.0115	2.90
FLH - PLH Crystallization Coef., Btu/hr/in <sup>2</sup> /F (W/m <sup>2</sup> /K)	0.1346	33.96
PLH - FZH Crystallization Coef., Btu/hr/in <sup>2</sup> /F (W/m <sup>2</sup> /K)	0.0250	6.30
Time from die to FLH, sec	5.94	5.94
Time from die to cone, sec	4.731	4.73
Time from cone to CLH, sec	0.972	0.97
Time from CLH to FLH, sec	0.24	0.24
FTR (process/polymer)	29.73	29.73
Internal Bubble Pressure, inch of H2O (Pa)	0.1145	28.52
Crystallization Rate, 1/sec	4.66	4.66
F <sub>net</sub> Lb, (N)	7.27	32.34
F <sub>air</sub> Lb, (N)	4.01	17.83
F <sub>net</sub> Lb, (N)	4.85	21.58
Force Vector, Psi (N)	9.62	42.77
Force Vector MD angle	28.87	28.87
Force Vector CD angle	56.28	56.28
Force Vector ND angle	50.44	50.44
Stress at die, psi (MPa)	1.45	0.0100

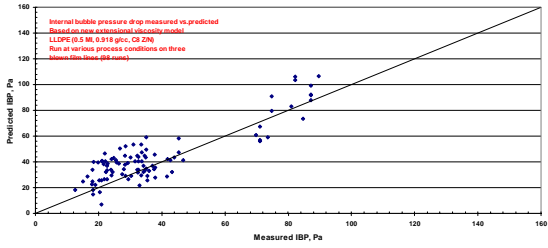
26

### Linear Regression Model

- Relaxation time ( $\lambda_e$ ) used was extensional relaxation time
- Residual stresses calculated using ( $\lambda_e$ )
- Crystallization time was calculated using CLH – FZH
- Bubble shape was calculated
- Bubble velocity was calculated
- Bubble temp profile was measured
- Bubble IBP was measured
- Resultant force were calculated
- Resultant force angles were calculated

27

### IBP: Measured vs. Predicted



28

### Impact & Elmendorf Tear

Property	Dart Impact	MD Elmendorf Tear	CD Elmendorf Tear
R <sup>2</sup>	0.8915	0.9072	0.9655
	Intercept	Intercept	Intercept
	Film Thickness	Output	Melt Temp
	BUR	Die gap	Film Thickness
	DDR	Melt Temp	BUR
	Die ^2	FLH	Sp Output
	FLH^2	FLH	Nusselt
	BUR^2	BUR	FTR
	FZH	DDR	ND direction angle
	MD Residual Stress	Out ^2	
	CD Residual Stress	Die ^2	
	Die - FLH U	FLH^2	
	PLH - FZH C	cone diameter	
	Fmd	Aspect Ratio	
	Fcd	Nusselt	
		Weissenberg CD	
		Die - FLH U	
		Internal Bubble Pressure	
		Fcd	
		MD direction angle	
		ND direction angle	
		(Die gap)*(BUR)	
		(Die gap)*(DDR)	
		(Output)*(Die gap)	

29

### MD Tensiles and Shrink

Property	MD 1% Sec Mod	MD Elongation	MD Shrink	MD Ultimate Tensile	MD Yield
R <sup>2</sup>	0.7891	0.988	0.8737	0.8951	0.8196
	Intercept	Intercept	Intercept	Intercept	Intercept
	Melt Temp	Die gap	Film Thickness	Melt Temp	BUR
	BUR	Film Thickness	BUR	Film Thickness	DDR
	Sp Output	DDR	DDR	DDR	Shear rate
	Gap^2	Gap^2	Weissenberg CD	DDR^2	MD Strain rate
	CD Strain rate	PLH	X	cone diameter	MD Residual Stress
	MD Residual Stress	Temp at cone	Fmd	MD Strain rate	Reynolds
	CD Residual Stress	Melt Velocity	(BUR)*(DDR)	Process Time	Nusselt
	Weissenberg MD	MD Residual Stress		Weissenberg MD	FTR
	FTR	(Film Thickness)*(DDR)		Weissenberg CD	Force Vector
	Internal Bubble Pressure			FLH - PLH C	(BUR)*(DDR)
	MD direction angle			Internal Bubble Pressure	
	CD direction angle			X	
	Ext. Stress at die			Force Vector	
				MD direction angle	
				Ext. Stress at die	
				(Film Thickness)*(DDR)	

30



### CD Tensiles

Property	CD 1% Sec Mod	CD Elongation	CD Ultimate Tensile	CD Yield
R <sup>2</sup>	0.849	0.605	0.8063	0.8438
Intercept	Intercept	Intercept	Intercept	Intercept
Die gap	Die gap	Film Thickness	Melt Temp	Die Diameter
Film Thickness	Film Thickness	Shear Stress	DDR	DDR
DDR	DDR	Deborah	cone diameter	FLH*2
Sp Output	Sp Output	PLH - FZH C	Shear rate	DDR*2
DDR*2	DDR*2		Melt Velocity	cone diameter
cone diameter	cone diameter		Process Time	Temp at cone
MD Strain rate	MD Strain rate		Nusselt	Shear rate
Process Time	Process Time		Die - FLH U	Melt Velocity
MD Residual Stress	MD Residual Stress		CLH - FLH C	FTR
CD Residual Stress	CD Residual Stress		Fcd	Internal Bubble Pressure
Reynolds	Reynolds		Force Vector	Fcd, N
Aspect Ratio	Aspect Ratio		MD direction angle	Force Vector
Weissenberg MD	Weissenberg MD		ND direction angle	ND direction angle
Internal Bubble Pressure	Internal Bubble Pressure			
Fmd	Fmd			
MD direction angle	MD direction angle			
(Die gap)/(DDR)	(Die gap)/(DDR)			

31

---

---

---

---

---

---

---

---

---

---

---

---

### Optical Properties

Property	Haze	20 Gloss	45 Gloss	Clarity
R <sup>2</sup>	0.787	0.895	0.8587	0.8119
Intercept	Intercept	Intercept	Intercept	Intercept
Die gap	Die gap	Melt Temp	Melt Temp	Die gap
Melt Temp	Melt Temp	FLH	Film Thickness	Melt Temp
Film Thickness	Film Thickness	DDR	BUR	FLH
FLH	FLH	Sp Output	DDR	BUR
BUR	FLH*2	FLH	Sp Output	DDR
DDR	FLH	FZH	Die *2	DDR*2
Gap*2	FZH	Temp at cone	Gap*2	MD Strain rate
BUR*2	Temp at cone	MD Residual Stress	BUR*2	Process Time
DDR*2	MD Residual Stress	Weissenberg CD	cone diameter	Die - FLH U
cone diameter	Weissenberg CD	Die - FLH U	CLH	FTR
CLH	Die - FLH U	FLH - PLH C	PLH	Fcd, N
FZH	FLH - PLH C	PLH - FZH C	FZH	Fmd
Temp at cone	PLH - FZH C	Temp at cone	Temp at cone	(Die gap)/(BUR)
MD Residual Stress	FTR	CD Strain rate	(FLH)/(DDR)	
CD Residual Stress	Internal Bubble Pressure	Process Time to FLH	(BUR)/(DDR)	
Deborah	Crystallization Rate	CD Residual Stress		
Weissenberg CD	Fmd	Aspect Ratio		
CLH - FLH C	Ext. Stress at die	Weissenberg CD		
FLH - PLH C	(FLH)/(DDR)	Die - FLH U		
PLH - FZH C		FLH - PLH C		
FTR		PLH - FZH C		
X'		X'		
Fmd		MD direction angle		
Force Vector		ND direction angle		
CD direction angle		(BUR)/(DDR)		
(Die gap)/(BUR)				
(BUR)/(DDR)				

32

---

---

---

---

---

---

---

---

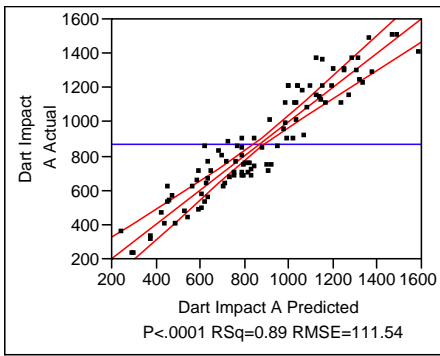
---

---

---

---

### Dart Impact (A)



33

---

---

---

---

---

---

---

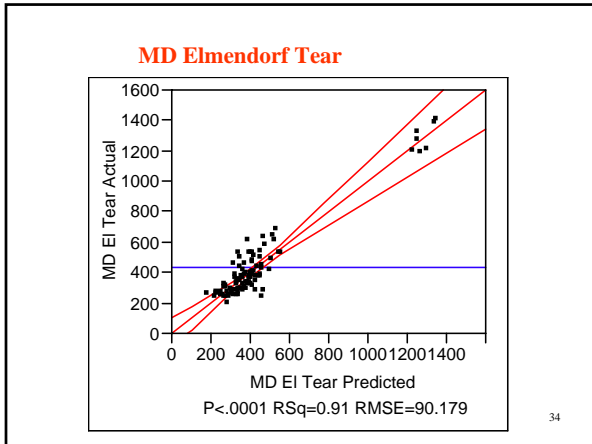
---

---

---

---

---




---

---

---

---

---

---

---

---

---

---

- Linear Model Summary**
- R<sup>2</sup> values for all film properties are fair to good
  - R<sup>2</sup> values for MD tear and impact are good
  - Model uses primary variables as input
  - Model calculates secondary variables
  - Primary and secondary variables are used to predict film properties
- 35

---

---

---

---

---

---

---

---

---

---

- Summary**
- P-P-P
    - Polymer – Intrinsic characteristics
    - Process - Fabrication variables
    - Properties - Orientation/ Relaxation & Crystallinity
  - Conventional variables do not describe process
  - Identified many key blown film process variables
  - Correlation of these variables can be made to film properties.
- 36

---

---

---

---

---

---

---

---

---

---



Thank You

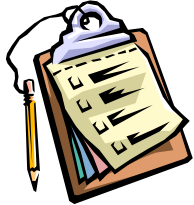
PRESENTED BY

**Thomas I. Butler**

Owner

**Blown Film Technology, LLC**

tbutler@blownfilmtech.com



*Please remember to turn  
in your evaluation sheet...*

37

---

---

---

---

---

---

---

---